Visual Comput (2006)
DOI 10.1007/s00371-006-0377-8

ORIGINAL ARTICLE

**Chunxia Xiao**
**Yongwei Miao**
**Shu Liu**
**Qunsheng Peng**

# A dynamic balanced flow for filtering point-sampled geometry

Published online: 28 February 2006


C. Xiao (✉) · Y. Miao · S. Liu · Q. Peng
State Key Lab of CAD & CG,
Zhejiang University,
310027, Hangzhou, China
{cxxiao, miaoyw, liushu,
peng}@cad.zju.edu.cn

**Abstract** 3D point data acquisition has become a practical approach for generating complex 3D shapes. Subsequent smoothing or denoising operations on these raw data sets are required before performing sophisticated modeling operations. Based on covariance analysis and constructed directional curvature, a new approach of anisotropic curvature flow is developed for filtering the point data set. By introducing a forcing term, a balanced flow equation is constructed, which allows the anisotropic diffusion flow to be restricted in the flow diffusion band of the original surface. Thus, the common problem of shape shrinkage that puzzles most current denoising approaches for point-sampled geometry is avoided. Applying dynamic balance techniques, the equation converges to the solution quickly with appealing physical interpretations. The algorithms operate directly on the discrete sample points, requiring no vertex connectivity information. They are shown to be computationally efficient, robust and simple to implement.

**Keywords** Covariance analysis · Point-sampled geometry · Filtering · Anisotropic diffusion flow · Dynamic balanced flow

## 1 Introduction

3D-scanning devices, such as laser-range scanners and structured light scanners, have been major sampling tools for acquiring digital 3D shapes of a complex surface. Despite the steady progress in accuracy, most available scanning devices still suffer from severe scanning artifacts, such as noise, outliers, holes, and even ghost geometry. The acquired raw point clouds thus need to be post-processed [25]. Similarly, shapes extracted from volume data obtained by MRI or CT devices often contain a significant amount of noises. In addition to those noises produced in the 3D shape acquisition step, some modeling operations on the point-sampled geometry may also introduce additional noises or undesirable artifacts. All these situations make denoising an inevitable operation before performing subsequent sophisticated geometry processing. In this paper, we focus on developing smoothing and denoising techniques on the point-sampled geometry.

It is widely recognized that an applicable denoising algorithm for a point-based surface should possess the following properties: (1) feature preservation: prominent shape features such as edges and corners of a surface should not be blurred. (2) Anti-shrinkage: the denoised shape should maintain the shape volume as before without manifest shrinkage. (3) Anti-point drifting: points should keep close to their original positions without noticeable drift on the surface, otherwise this may cause non-uniform sampling densities ultimately leading to holes on the surface.

To develop such an algorithm, we employ a balanced flow equation on the point-sampled geometry. Note that the traditional approaches of fairing point-sampled surfaces via PDEs can hardly be adopted here, as no vertex connectivity information among the discrete points is

available. The geometric attributes of the surface, such as curvature, cannot be determined analytically on the point set surface due to the lack of explicit surface representation. We propose the following techniques to overcome these difficulties.

- Based on the covariance analysis and the efficiently constructed directional curvature, we develop a well-posed anisotropic curvature flow allowing prominent surface features and other details of the objects to be treated in different ways.
- By introducing a forcing term, we construct a balanced flow equation on the point-sampled geometry, so as to restrict the anisotropic curvature flow in the flow diffusion band of the original surface, thus shrinkage is avoided.
- By applying a dynamic balance computation mechanism, the equation converges to the solution quickly with appealing physical interpretations.

Various smoothing operators, such as the curvature flow smoother, the anisotropic smoother, the volume-preserved flow smoother, and the balanced flow smoother are developed for filtering the point-based geometry according to the requirements of various corresponding applications.

### 1.1 Related work

A variety of smoothing algorithms have been proposed for meshes in recent years, please refer to [6, 7, 9] and the references therein. There are relatively few methods on fairing the point-sampled geometry, however. One of the most common techniques for fairing and denoising of surfaces is based on Laplace smoothing. Using a discrete approximation to the Laplacian, Taubin [21] introduced the techniques of signal processing to surface fairing. Observing that fairing surfaces can be performed in the normal direction, Desbrun et al. [5] introduced geometric diffusion algorithms for meshes. Based on the umbrella operators given in [5], Pauly et al. [18] proposed a multilevel smoothing operator for point-based geometry. A tedious problem of iterative smoothing operators is volume shrinkage. To avoid shape shrinkage in smoothing the point-sampled geometry, Pauly et al. [18] measured the shrinkage locally and displaced neighbors to compensate the shrinking volume. While this method is isotropic, some important geometric features are blurred. By constructing local finite matrices over small point neighborhoods and assembling these matrices in a single matrix, Clarenz et al. [3, 4] discretized and solved an anisotropic geometric diffusion equation for fairing a point set surface. More recently, by extending Taubin's work [22] on the curvature tensor of polyhedral meshes to purely point-sampled geometries, Lange and Polthier [12] presented an anisotropic fairing algorithm that incorporated the principal curvature information.

Other methods have also been proposed for fairing the point set surface. By establishing a concept of local frequencies on geometry, Pauly et al. [15] presented a versatile spectral representation that provides a rich repository of signal processing algorithms for point-sampled geometry. Alexa et al. [1] proposed a moving least squares (MLS) method to fit a point set with a local polynomial approximation; the point set surface can be smoothed by shifting point positions towards the corresponding MLS surface. To construct the MLS surface, a non-linear minimization problem has to be solved. Fleishman et al. [6] described a mesh smoothing algorithm based on the idea of bilateral filtering for gray and color images [24]. To adopt this method to fair the point-based geometry, the normal vector at each point has to be estimated during each smoothing step. Based on the same bilateral filtering model [24], Jones et al. [9] presented a non-iterative, feature preserving filtering technique applicable to an arbitrary "triangle soup". Their method estimated the new position of each vertex based on the predictions from its spatially near triangles. While this method obtained impressive results in mesh smoothing, a direct extension of the method to the point set surface does not work as satisfactorily as expected. Soon after, Jones et al. [10] proposed a bilateral filter-based method for denoising normals of point models. In a concurrent work, Schall et al. [20] developed a method based on a kernel density estimation technique to filter the noisy point set sampled from a smooth surface.

## 2 Well-posed anisotropic flow

Smoothing is an elementary editing operation. It can be applied to reduce noise, to smooth out high frequency details, such as ripples and spikes, or to soften creases occurring during the editing process. In this section, we introduce a curvature flow smoother for the point-sampled geometry.

### 2.1 Covariance analysis

Covariance analysis upon the neighborhood of the centroid of a point cloud can be used to estimate various local surface properties, such as the normal vector and curvature [8, 16, 17, 26]. The covariance matrix of the point cloud is defined as

$$C = \begin{bmatrix} p_{i_1} - \bar{p} \\ \cdots \\ p_{i_k} - \bar{p} \end{bmatrix}^T \cdot \begin{bmatrix} p_{i_1} - \bar{p} \\ \cdots \\ p_{i_k} - \bar{p} \end{bmatrix}, \tag{1}$$

where $p_{i_k}$ is the $k_{th}$ neighboring point around $p_i$ and $\bar{p}$ is the centroid of the neighborhood. Since $C$ is symmetric and positive semi-definite, all eigenvalues $\lambda_i (i = 0, 1, 2)$ are of real value and the eigenvectors $v_i (i = 0, 1, 2)$ form an orthogonal basis. The eigenvalue $\lambda_i$ measures the varia-

tion of the local point set along the direction of the corresponding eigenvector.

If we assume that $\lambda_0 \le \lambda_1 \le \lambda_2$, let the plane $(x-\bar{p})\cdot v_0 = 0$ minimize the sum of the squared distance between the plane and the neighboring points $p_i$ as illustrated in Fig. 1(a), then the normal $v_0$ of this plane can be regarded as the normal of local surface at $p_i$. In this particular case, the eigenvalue $\lambda_0$ expresses the variation of the surface along the normal $v_0$, in other words it estimates how much the sample points of the surface deviate from the tangent plane. Pauly et al. [16] defined

$$\sigma_n^i = \sigma_n(p_i) = \frac{\lambda_0}{\lambda_0+\lambda_1+\lambda_2} \tag{2}$$

as the surface variation at point $p_i$ assuming a neighborhood of size $n$. It is also observed that surface variation $\sigma_n(p_i)$ is closely related to the local curvature. Its value depends on the size of the neighborhood. To ensure a consistent orientation of the normal vectors, we use a method based on the minimum spanning tree, as described in [8].

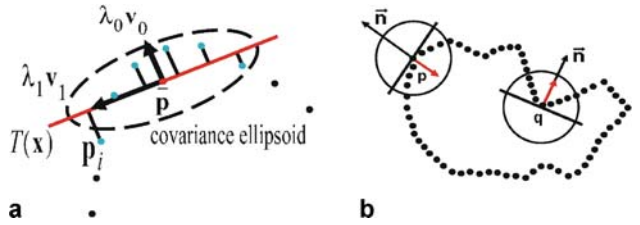


**Fig. 1. a** Covariance analysis. **b** Determining the sign of the curvature normal

## 2.2 Curvature flow

With the normal $v_0$ and the curvature $\sigma_n$ for each point $p_i$ on the point set surface, we can now define a curvature flow equation on the point set surface. The basic idea of defining such a diffusion flow is to allow the point moving along the normal with a speed equal to the curvature $\sigma_n$ as shown in Fig. 1(b). Since the point is moved along the normal direction, the proposed curvature flow will not introduce undesirable points drifting over the surface.

One problem is how to define the sign of the diffusion direction, that is, how to determine the sign of the curvature, as illustrated in Fig. 1(b). Assuming that index set $N(p_i)$ is the $k$-nearest neighbor around the point $p_i$, the sign of curvature can be determined by the following formulation

$$\text{Dire} = \frac{\sum_{u\in N(p_i)} G(\|p_i-u\|)(n_i,\, p_i-u)}{\sum_{u\in N(p_i)} G(\|p_i-u\|)}, \tag{3}$$

where $n_i$ is the estimated surface normal at the point $p_i$, $G(x)$ is the standard Gaussian filter $e^{-x^2/2\sigma^2}$ and $\sigma$ is a parameter controlling the individual contribution of the sample points in the neighborhoods $N(p_i)$. If Dire $\ge 0$, then sign $= 1$, else sign $= -1$. We define the directional curvature $\bar{k}_i$ as $\bar{k}_i = \text{sign}\cdot\sigma_n^i$. The formulation in Eq. 3 dynamically adapts the local sampling density and is stable and efficient for noisy surface.

The curvature flow equation on point-sampled geometry is then expressed as follows

$$\frac{\partial u_i}{\partial t} = -\bar{\kappa}_i n_i, \quad \bar{k}_i = \text{sign}\cdot\sigma_n^i. \tag{4}$$

The normal $n_i$ can be evaluated by the following steps. First, we adopt the covariance analysis to get eigenvector $v_0$, let $n_i'$ be the corresponding normal of point $p_i$ at the previous smoothing step, if $v_0\cdot n_i' \ge 0$, then $n_i = v_0$, else $n_i = -v_0$. Since during each diffusion iteration the variation of the normal directions at each point is small, we can get the right result. Thus the time-consuming process of keeping consistent orientation of the normal vectors using a minimum spanning tree is avoided during each iteration.

If $\sigma_n(p) = 0$, all points lie on the plane. This is compared with the Laplacian of the surface at a point, which has both normal and tangential components, even if the surface is locally flat, the Laplacian approximation will rarely be the zero vector [11].

The curvature flow Eq. 4 is an isotropic smoother as shown in Figs. 2(b) and 2(c). It is motivated by the mean curvature flow operator [5] defined on meshes, where a robust curvature flow operator is defined based on the 1-ring neighbors $N_1(i)$ of vertex $v_i$ employing the vertex connectivity information.

## 2.3 Well-posed anisotropic flow

In the preceding section, we presented a curvature flow equation for smoothing a point set surface. As the curvature flow is an isotropic smoother, the prominent surface features and other details of the objects might be smoothed out without discrimination. In this subsection, we develop an anisotropic flow allowing prominent features and other details of the surface to be treated in different ways.

Motivated by the nonlinear diffusion method proposed in [19], we modify the diffusion coefficient at features and change Eq. 4 into the following model:

$$\frac{\partial u_i}{\partial t} = -g(|\bar{\kappa}_i|)\bar{\kappa}_i n_i, \tag{5}$$

where $g(x) \ge 0$ is a non-increasing function. Here we set $g(x) = 1/(1+K\times x^2)$ and $K$ is a parameter that can be tuned by the user to control the diffusion speed.

Unfortunately, the above anisotropic curvature flow Eq. 5 cannot not produce satisfactory results when dealing with a seriously noisy surface, as illustrated in Fig. 4(c). As observed in Eq. 5, the diffusivity coefficient $g(|\bar{\kappa}_i|)$ is used not only for geometric feature detection but also for controlling the diffusion speed. Since it is difficult to discriminate the noise point and the feature point on

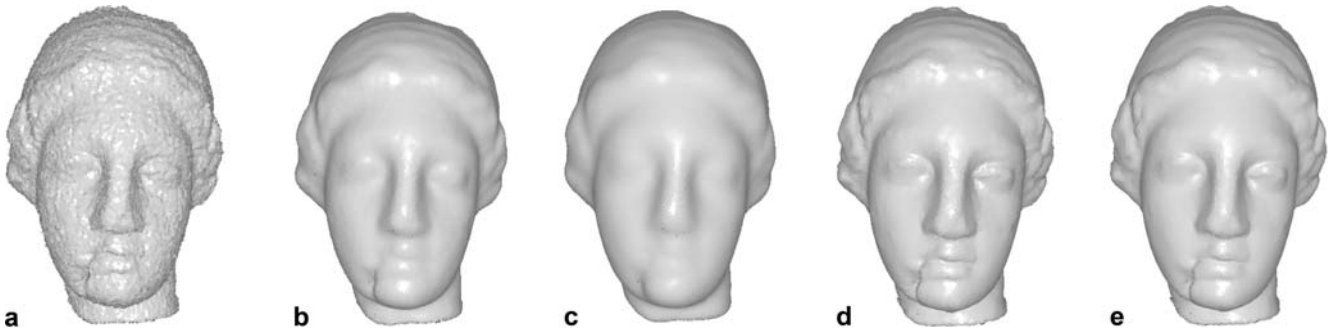


**Fig. 2. a** Corrupted model. **b**, **c** Curvature flow applied on the noised point-sampled geometry, producing a sequence of diffused point set surface. **d** Well-posed anisotropic flow performed on (**a**); note the manifest volume shrinkage. **e** Volume-preserved flow performed on (**a**)

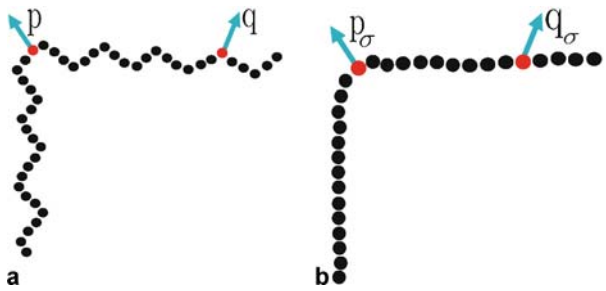


**Fig. 3. a** Original noised curve. **b** Smoothed curve. The diffusivity coefficient defined on the smoothed surface is more accurate

the noisy surface, we define the diffusivity coefficient on an alternative filtered surface that can faithfully respect the prominent features of the original surface as shown in Fig. 3(b). We apply the Gaussian filter to pre-filter the current surface $M$ and evaluate the curvature $\kappa_H$ of the filtered surface $M_\sigma$ using the covariance analysis methods, where $\sigma$ denotes the Gaussian filter width. By substituting $|\bar{\kappa}(u)|$ with $|\kappa_H(G_\sigma \times u)|$, we present the following well-posed anisotropic flow equation.

$$\frac{\partial u}{\partial t} = g(|\kappa_H(G_\sigma \times u)|)(-\bar{\kappa}n), \tag{6}$$

where $G_\sigma$ is a Gaussian convolution kernel and the term $|\kappa_H(G_\sigma \times u)|$ is the local estimate of $|\bar{k}(u)|$, which is used for noise elimination. The term $g = g(|\kappa_H(G_\sigma \times u)|)$ is used for geometric feature detection and it controls the diffusion speed. Using the well-posed anisotropic model, prominent features like boundaries are preserved, while noisy and homogeneous regions will be smoothed as shown in Fig. 4(d).

A similar technique for determining normals based on a smoothed shape is also used in [9, 13, 23]. Since the normals are first-order properties of the mesh, they are usually more sensitive to noises than vertex positions. Jones et al. [9] mollified the estimators by smoothing the normals, which corresponded to a simple Gaussian smoothing.

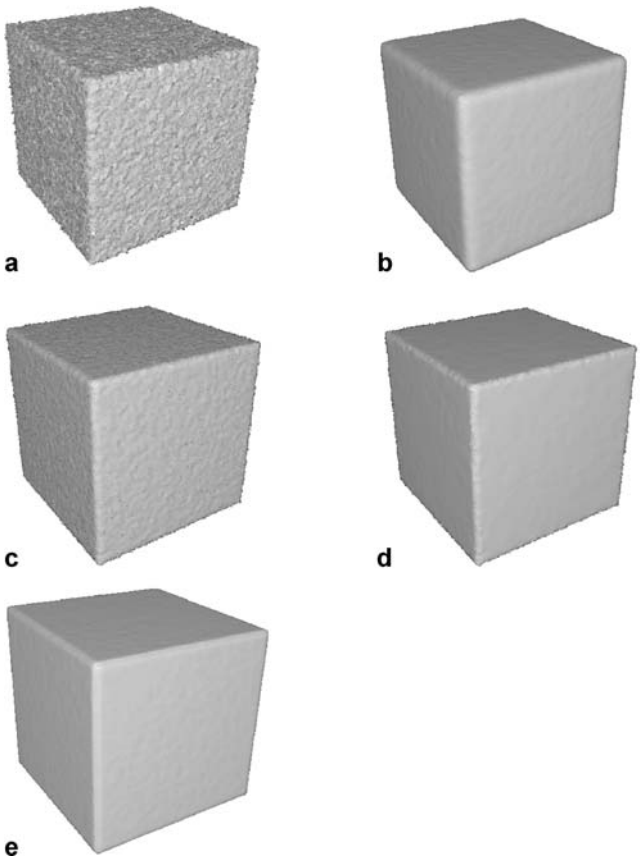


**Fig. 4. a** Corrupted model. **b** Curvature flow method. **c** Naive anisotropic flow. **d** Well-posed anisotropic flow

## 3 Balanced flow equation

A tedious problem of iterative smoothing operators is volume shrinkage. Taubin [21] resolved this problem by alternating between smoothing steps with positive and negative scale parameters. Desbrun et al. [5] measured the object volume before and after the smoothing operation and

rescaled the model uniformly. Nevertheless, it is difficult to evaluate the volume of the point-sampled geometry. Moreover, the rescale technique is a global operation, whereas denoising is a local operation, thus the global rescale techniques will cause model distortion during the iterative smoothing operations, as shown in Fig. 1 in Pauly et al. [18]. To deal with this problem, Pauly et al. [18] measured the shrinkage locally and displaced neighbors to compensate the shrinking volume. In this section, we present a more elaborate method with appealing physical interpretations to eliminate the shrinkage.

### 3.1 Volume-preserved flow

Motivated by the "well-balanced flow equation" [2], where the term $(I-u)$ has the property of preserving $u(x, y, t)$ close to the initial image $I(x, y)$, we introduce a forcing term $(I-u)$ to the well-posed flow and propose the following equation:

$$\frac{\partial u}{\partial t} = g(|\kappa_H(G_\sigma \times u)|)(-\bar{\kappa}n) + (I-u). \tag{7a}$$

Since our interest is in the steady state solution, the initial condition of the above equation can be replaced by an arbitrary initial condition

$$u(x, y, z, 0) = \chi(x, y, z). \tag{7b}$$

In our experiments, we take $u(x, y, z, 0) = I(x, y, z)$. The steady state of this initial value problem is a solution of following equation:

$$u = I + g(|\kappa_H(G_\sigma \times u)|)(-\bar{\kappa}n). \tag{8}$$

We call Eqs. 7a and 7b the "volume-preserved flow". The solutions of the volume-preserved flow model are well-behaved in that they do not stray too far away from the original mesh surface $I$, unless forced by the initial condition $\chi$, even then they eventually approach the range of $I$ as $t \to \infty$.

Intuitively, the forcing term $I-u$ has the effect of locally moderating the diffusion as surface $u$ diffuses further away from the original mesh $I$. The following physical interpretation of this initial value problem further confirms this belief: let $\Omega$ be a thin anisotropic annular solid of some material resting on top of another solid $\Omega_0$ of another material, as in Fig. 5(a). Suppose that the space and time varying thermal conductivity of $\Omega$ is given by $ag$, where the constant $a$ is the coefficient of heat transfer between $\Omega$ and $\Omega_0$. If the initial temperature at each point of $\Omega$ is given by $\chi(x, y, z)$, then $u$ represents the space and time varying temperature of $\Omega$. The temperature distribution of $\Omega_0$ is fixed with the value $I$. Therefore, the solution $u$ is guaranteed to be a faithful approximation of the original surface function $I$. The forcing term $I-u$ performs the role of drawing the anisotropic diffused $u$ back to $I$.

To confirm the belief that the solution $u$ of Eqs. 7a and 7b converges to a faithful approximation of the original surface $I$, we give a special example as illustrated by Fig. 6. Let $M'$ be a corrupted model of the original surface $M_0$ by adding random noise. The initial value $\chi$ in Eq. 7b is replaced by $M'$, and $I$ is substituted by $M_0$. Our experiment shows that the solution $u$ converges to $M_0$, as shown in Fig. 6(e). Let $p$ be a point on the original surface $M_0$, and $p'$ be its corresponding vertex on the solution $u$. Let $\text{dist}(p_i, p_i')$ be the distance error between $p_i$ and $p_i'$ and $E(u, M_0) = \sum_{i=0}^{N} \text{dist}(p_i, p_i')/N$ the average distance error. The radius of the bounding box of the Venus model is 24.20, the average distance error $E(u, M_0)$ is 0.12.

From the volume-preserved flow Eqs. 7a and 7b, we can draw the conclusion that the solution of interest $u$ con-

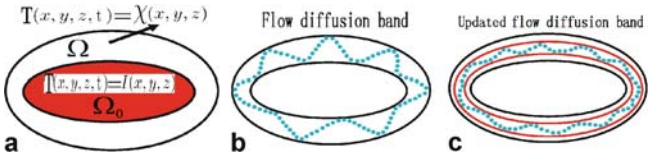


**Fig. 5.** **a** Physical models of the volume-preserved flow equation. **b** The flow diffusion band of the original surface. **c** Dynamically updated flow diffusion band

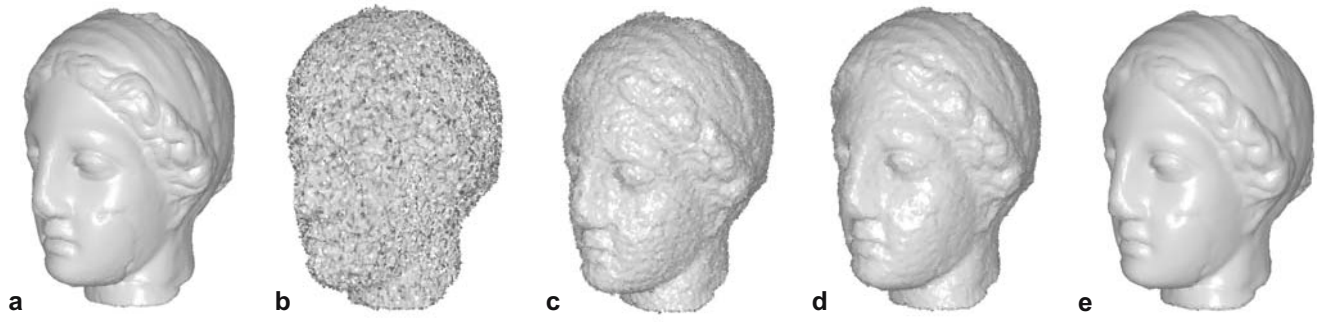


**Fig. 6a–e.** Converged well-posed model. **a** Original Venus model $M_0$. **b** Corrupted model $M'$. The original surface $I$ is substituted by $M_0$, initial value $\chi$ is substituted by $M'$ . The solution $u$ converges to $M_0$ as shown in **e**. **c**, **d** Successive immediate results

verges and is restricted in the flow diffusion band $B$ of the original surface $I$, as illustrated in Fig. 5(b). The solution $u(x, t)$ is an estimated surface whose range is contained inside that of the original function as following.

$$\inf_{\xi \in B} I(\xi) \leq u(x, t) \leq \sup_{\xi \in B} I(\xi) \quad \forall x \in B \ \text{ for any } \ t < \infty.$$

Therefore, a high feature-preserved performance can be obtained as well as anti-shrinkage, as shown in Fig. 2(e).

### 3.2 Dynamic volume-preserved flow

From the discussion in the previous section, we know that the volume-preserved flow is a well-founded equation; it brings the anisotropic diffusion method an appealing sense of optimality. As an optimality process, the converging rate is manifest at the first iterations, while the equation then converges to the solution slowly. For models with relative low noise, satisfactory results can be achieved with several iterations, whilst to deal with a corrupted model with heavy noises, it needs to find a more effective and efficient computation scheme.

We introduce a dynamic flow algorithm to resolve this problem. The key ingredient of the technique is that instead of setting $I$ as the fixed original surface value $M$, we dynamically update $I$ with the immediate generated solution $u$. After every $L$ iterations we achieve the immediate fairing surface $U_L$, then the original $I$ is substituted by $U_L$, and the iteration process then continues. With several such repetitions satisfactory results are achieved. This computation scheme presents advantages thereinafter: the balanced state is dynamically broken, the original $I$ is dynamically updated, and the flow equation converges to the solution quickly. The other motivation to apply this technique is that when dealing with severely corrupted models it is not optimal to always preserve the solution $u$ close to the original surface $I$. To dynamically update the original $I$ with the new generated $U_L$ surface after several iterations would be a better choice. The anisotropic flow equation will be performed in a thinner flow diffusion band $B'$, that is, the flow diffusion band $B$ is also updated dynamically according to the dynamically updated $I$. As the updated band $B'$ is still contained in the original band $B$, the volume shrinkage is naturally prevented, as shown in Fig. 5(c).

Our experiments also show that the above computation scheme can attain satisfactory performance when denoising heavily noised models. As shown in Fig. 7(b), the face of a cube model cannot be smoothed flat even after 200 iterations using volume-preserved flow. While this dynamical flow algorithm requests only 12 iterations with $L = 4$ to obtain the desirable result.

### 3.3 Balanced flow

Although the preceding volume-preserved flow model successfully resolves the shrinkage problem, according to Eqs. 7a, 7b, anisotropic curvature flow cannot work well in the diffusion band B. The reason is that all the points are pulled back to their position without distinction, To selectively apply the anisotropic curvature flow on the point set surface, we improve Eq. 7 further by adding a moderated selector

$$\frac{\partial u}{\partial t} = g \cdot (-\bar{\kappa} n) + (1 - g) \cdot (I - u), \tag{9}$$

where $g = g(|\kappa_H(G_\sigma \times u)|)$ and $(1 - g)$ works as a moderated selector of the diffusion process. We call the above equation the "balanced flow model". This model is capable of forcing point-set surfaces close to the initial surface $I$ in the feature areas where $g \to 0$. On the other hand, in homogeneous areas where $g \to 1$, the forcing term will have a weak effect, which allows for a finer detail smoothing.

This simple change to the volume-preserved flow model preserves the feature better comparing with the volume-preserved flow, meanwhile preventing the volume shrinkage, as shown in Fig. 8(d). Both Figs. 8(c) and 8(d) undergo the same number of iterations. Table 1 lists the pseudocode of the proposed model.

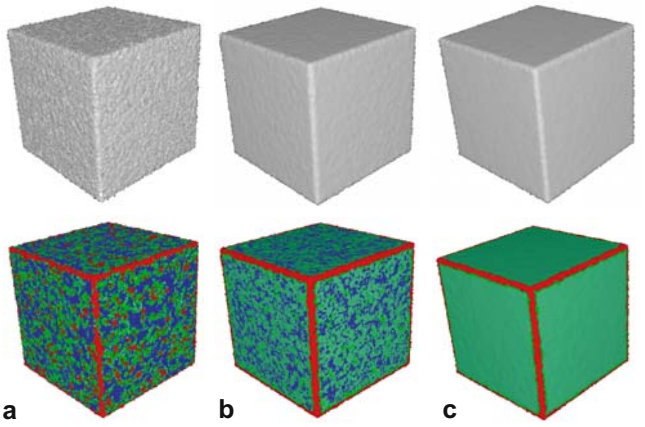


**Fig. 7a–c.** Dynamic volume-preserved flow equation. **a** Original cube model. **b** Volume-preserved flow equation. **c** Dynamic volume-preserved method. The *bottom row* is a curvature visualization of the *top row*

**Table 1.** The pseudocode of the balanced flow equation for smoothing point set surface

```
Balanced flow filtering(I, K, σ, N, s)
    Let M_ini = I;
    For (steps = 1 ... N)
        I' = Gauss_σ(I);
        For each point v'_i in I'
            Compute κ'_H for each point on I' ;
        For each point v_ini,i in I
            v_i = v_i + s * (g_k(κ'_H) * (−κ̄n) +
                  (1 − g_k)(κ'_H) * (v_ini,i − v_i));
    Return I
```

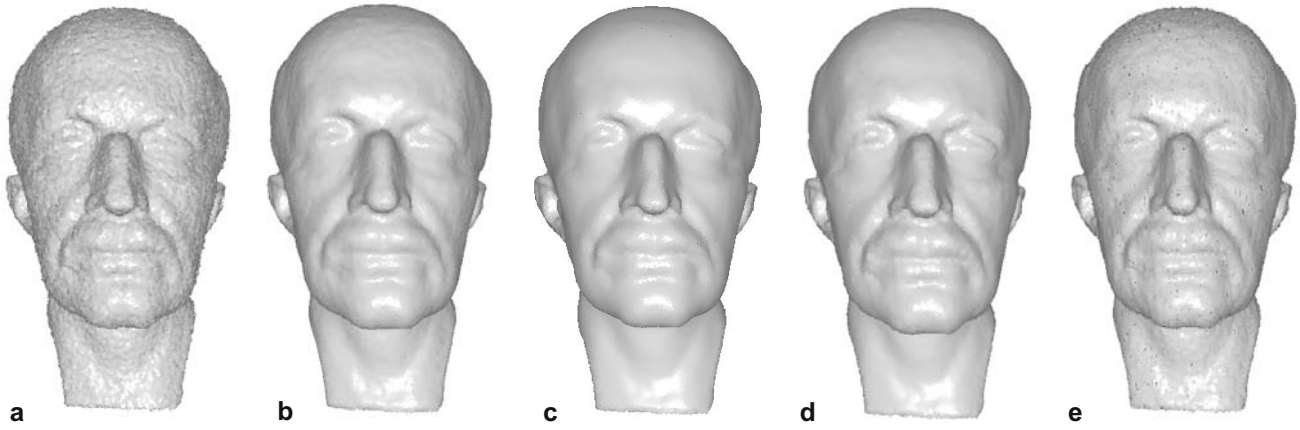


**Fig. 8.** **a** Corrupted Plank model with noise. **b** Bilateral filtering. **c** Volume-preserved flow. **d** balanced flow. **e** Non-iterative method without area weight. All **b**, **c**, **d** and **e** are computed using the neighborhoods of the same size

Table 1 shows the balanced flow method for smoothing point set surface. The corresponding parameters are: $I$ is the original point set surface, $K$ is threshold value for curvature flow used for feature detection, $\sigma$ is the filter width used in Gauss filtering, $s$ is the step length, and $N$ is the number of smoothing steps.

## 4 Results and discussions

In this section, we demonstrate some experimental results of the balanced flow diffusion algorithm and compare them with results of other smoothing algorithms. The users can tune two parameters to control the performance.

The first parameter is the Gauss filter width $\sigma$, which plays the role of pre-filtering the surface to obtain more accurate curvature evaluation used for feature detection. To process a seriously noisy model, $\sigma$ is usually set to a relatively large value to capture the accurate features of the models.

The second parameter is a constant $K$ used in $g(x)$, which has dual roles. One is to allow the function $g(x)$ to play the role of a moderated selector to balance between the diffusion term and the forcing term, the other is to support the anisotropic diffusion. Note that $g(x) = 1/(1 + K \times x^2)$ is a non-increasing function. A different value of $K$ determines whether $g$ goes to 0 or 1, and its value needs to be changed every time a new model is smoothed. For example, to preserve or enhance prominent features such as the shape edges of a cube model, we would assign a relatively large value for the parameter $K$.

Figure 2(a) shows the original corrupted model $M_0$, Fig. 2(d) shows the result $M'$ of applying a well-posed anisotropic flow to $M_0$, while Fig. 2(e) is the result $M$ of applying volume-preserved flow. The radius of the bounding box of the Venus model is 24.20, the average distance error $E(M_0, M') = 1.2$ and $E(M_0, M) = 0.14$. The numerical results suggest that volume-preserved flow preserves the volume of the model well.

Figure 7 shows an example of dynamic volume-preserved flow. In this example, we choose $L = 4$, after 12 iterations we achieve the appreciated results, the perturbations are smoothed out and the face is smoothed into a flat plane. Let $M_0$ be the original model in Fig. 7(a), $M'$ (Fig. 7(d)) is the filtered result, the average distance error $E(M, M') = 0.18$, whereas the radius of the bounding box of the cube is 30.20.

In Fig. 8, we compare our method with the bilateral denoising method. Although the bilateral method was originally proposed for mesh denoising [6], it can also be adopted to denoise the point-sampled geometry provided that the surface normals at the points can be evaluated before each iteration. Figure 8(b) is the result of applying the bilateral denoising method, the normals were computed based on covariance analysis. There is an apparent volume shrinkage, since no volume preservation technique is incorporated. The features are enhanced in Fig. 8(d) by using the balanced flow. In both cases we adopt the same size of neighborhood. It takes four iterations using the bilateral denoising method, while our method takes 11 iterations with $L = 4$. Since the balanced flow diffusion tries to seek an optimal solution, our method usually takes more iterations.

One benefit of anisotropic diffusion is its ability to preserve edges and corners during iterations. By predicting the new position of a vertex $p$ based on the local geometry of its neighborhood, Jones et al. [9] derived a non-iterative feature-preserving filtering technique applicable to arbitrary "triangle soup". In addition to the spatial weight and the influence weight, Jones et al. [9] also included the weight regarding the area of the neighboring triangles to account for the sampling rate of the surface.

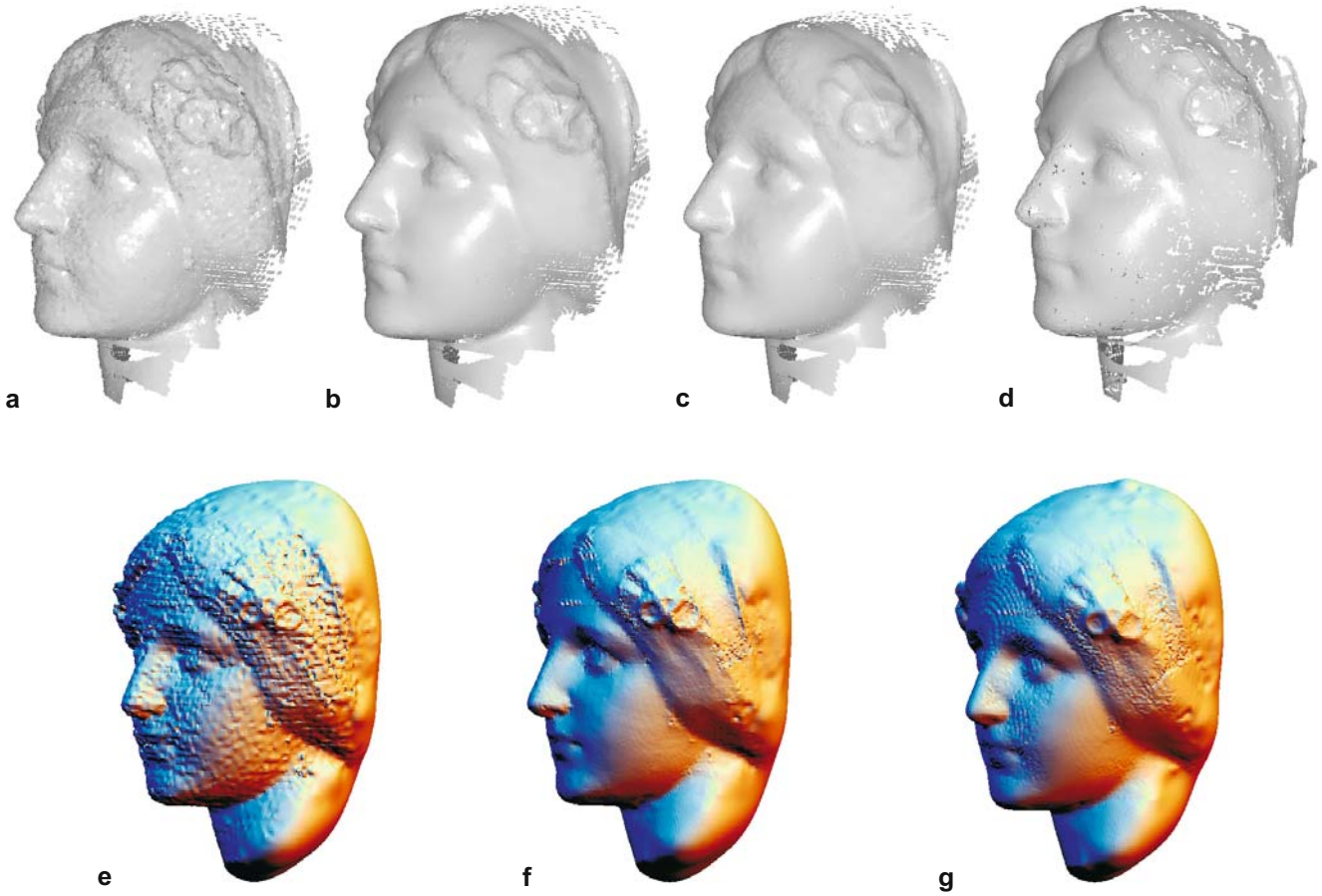


**Fig. 9. a** Real-world datasets using laser scanners. **b** Dynamic balanced flow. **c** Bilateral filtering. **d** Laplacian method. All **b**, **c** and **d** are computed using the same size of neighborhood. **e**, **f**, **g** are the surface reconstruction of **a**, **b**, **c** using compactly supported radial basis functions

Since no connectivity information among the neighboring points is provided in the point set surface, it is not convenient to compute the area weights and hence not straightforward to apply this method to point sampled geometry. If using only spatial and influence weights and letting all area weights be 1, as the point set surface is usually re-sampled uniformly, the predicted point will drift on the surface and generate some holes, as shown in Fig. 8(e). After abandoning area weights, the algorithm was extended to improve the evaluation of normal of the point set and obtained satisfactory rendering results [10].

Figure 9 demonstrates the result of applying our algorithm to real-world datasets acquired using laser scanners. We compare our method with the bilateral denoising method [6] and the Laplacian method [18]. The result shown in Fig. 9(b) is similar to that in Fig. 9(c), both results preserve the prominent features, while more hair details are revealed in Fig. 9(b). Moreover, more redundant details are smoothed away in Fig. 9(b). Note the small holes yielded due to the point drifting caused by the Laplacian method (Fig. 9(d)). Surface reconstruction is one of the most fundamental operations in digital geometry processing. However, many surface reconstruction approaches are sensitive to noise implied in the data set. Figures 9(e), (f) and (g) show the surface reconstruction results of (a), (b) and (c) using the multi-scale approach presented in [14] with the same set of parameter values in the software presented by Yutaka Ohtake et al.

## 5 Conclusion and future work

We have presented a novel approach for fairing point-sampled geometry taking the balanced flow equation as the theoretical foundation. The algorithm tries to find an optimal solution in the flow diffusion band of the original surface. Our algorithm has several mathematically desirable properties for achieving satisfactory performance, i.e., noise removal, feature preservation, anti-shrinking and anti-point drifting. Moreover, the proposed

algorithm is simple, practical and has appealing physical interpretations.

The size of the neighborhoods is important for estimating local shape attributes of the point set surface. In our experiments, all neighborhood sizes are set between 15 and 25. The investigation of an optimal neighborhood for each point on the point set surface is the subject of future work; Pauly et al. [17] have provided some ideas for choosing neighborhood sizes. While covariance analysis is useful for estimating local surface properties, it also has some drawbacks in dealing with sharp corners. Since the balanced flow diffusion has an optimal solution, we wish to find the ideal criterion for terminating the evolution of the partial differential equation based on the noise standard deviations.

**Acknowledgement** We would like to thank Yutaka Ohtake and Alexander Belyaev for making their surface reconstruction software available. Special thanks are due to Xiaomao Lin and Xin Xu for scanning the model in Fig. 9(a). This work was supported by the National Basic Research Program of China (No. 2002CB312101) and NSF of China (No.60503056).

## References

1. Alexa, M., Behr, J., Cohen-Or, D., Fleishman, S., Levin, D., Silva, C.T.: Point set surfaces. IEEE Visualization, pp. 21–28 (2001)
2. Barcelos, C., Boaventura, M., Silva, E.: A well-balanced flow equation for noise removal and edge detection. IEEE Trans. Image Processing **14**, 751–763 (2003)
3. Clarenz, U., Rumpf, M., Telea, A.: Fairing of point based surfaces. Computer Graphics International, Crete, Greece, IEEE CS Press, pp. 600–603 (2004)
4. Clarenz, U., Rumpf, M., Telea, A.: Finite elements on point based surfaces. Eurographics Symposium on Point-Based Graphics. Zurich, The Eurographics Association (2004)
5. Desbrun, M., Meyer, M., Schroer, P., Barr, A.: Implicit fairing of irregular meshes using diffusion and curvature flow. Proc. of ACM SIGGRAPH, pp. 317–324 (1999)
6. Fleishman, S., Drori, I., Cohen-Or, D.: Bilateral mesh denoising. Proc. of ACM SIGGRAPH, pp. 950–953 (2003)
7. Hildebrandt, K., Polthier, K.: Anisotropic filtering of non-linear surface features. Proc. of Eurographics, pp. 391–400 (2004)
8. Hoppe, H., DeRose, T., Duchamp, T., McDonald, J., Stuetzle, W.: Reconstruction from unorganized points. Proceedings of ACM SIGGRAPH, pp. 71–78 (1992)
9. Jones, T.R., Durand, F., Desbrun, M.: Non-iterative, feature-preserving mesh smoothing. Proc. of ACM SIGGRAPH, pp. 943–949 (2003)
10. Jones, T., Durand, F., Zwicker, M.: Normal improvement for point rendering. IEEE Comput. Graph. Applic. **24**(4), 63–56 (2004)
11. Kobbelt, L., Campagna, S., Vorsatz, J., Seidel, H.P.: Interactive multi-resolution modeling on arbitrary meshes. Proc. SIGGRAPH, pp. 105–114 (1998)
12. Lange, C., Polthier, K., Anisotropic fairing of point sets. Special Issue of CAGD (2005) ZIB-Preprint 05-16
13. Ohtake, Y., Belyaev, A., Bogaevski, I.: Mesh regularization and adaptive smoothing. Comput.-Aid. Des. **33**(11), 789–800 (2001)
14. Ohtake, Y., Belyaev, A., Seidel, H.P.: A multi-scale approach to 3D scattered data interpolation with compactly supported basis functions. Shape Modeling International, pp. 153–161, IEEE Computer Society (2003)
15. Pauly, M., Gross, M.: Spectral processing of point-sampled geometry. ACM SIGGRAPH, pp. 379–386 (2001)
16. Pauly, M., Gross, M., Kobbelt, L.: Efficient simplification of point-sampled surfaces. Proc. IEEE Visualization, pp. 163–170 (2002)
17. Pauly, M., Keiser, R., Gross, M.: Multi-scale feature extraction on point-sampled surfaces. Proc. of Eurographics, pp. 281–290 (2003)
18. Pauly, M., Kobbelt, L., Gross, M.: Multiresolution modeling of Point-sampled geometry. ETH Zurich Technical Report, http://graphics.stanford.edu/∼mapauly/Pdfs/MultiresModeling.pd (2002)
19. Perona, P., Malik, J.: Scale-space and edge detection using anisotropic diffusion. IEEE Trans. Patt. Anal. Mach. Intell. **12**(7), 629–639 (1990)
20. Schall, O., Belyaev, A., Seidel, H.P.: Robust filtering of noisy scattered point data. Eurographics Symposium on Point-Based Graphics. Stony Brook, New York, USA, Eurographics Association, pp. 71–77 (2005)
21. Taubin, G.: A signal processing approach to fair surface design. Proc. SIGGRAPH, pp. 351–358 (1995)
22. Taubin, G.: Estimating the tensor of curvature of a surface from a polyhedral approximation. ICCV, pp. 902–907 (1995) Computer Society, Washington, D.C.
23. Taubin, G.: Linear anisotropic mesh filtering. IBM Research Report RC2213 (2001)
24. Tomasi, C., Manduchi, R.: Bilateral filtering for gray and color images. ICCV, pp. 839–846 (1998), Bombay, India
25. Weyrich, T., Pauly, M., Heinzle, S., Keiser, R., Scandella, S., Gross, M.: Post-processing of scanned 3D surface data. Eurograpics Symposium on Point-Based Graphics, pp. 85–94 (2004)
26. Xiao, C., Zheng, W., Peng, Q., Forrest, A.R.: Robust morphing of point-sampled geometry. J. Comput. Anim. Virtual Worlds **15**(3–4), 201–210 (2004)




CHUNXIA XIAO was born in 1976 and is a Ph.D. candidate at the State Key Lab. of CAD & CG, Zhejiang University, People's Republic of China. His research interests include virtual reality, digital geometry processing and point-based computer graphics.

YONGWEI MIAO was born in 1971 and is a Ph.D. candidate at the State Key Lab. of CAD & CG, Zhejiang University, People's Republic of China. His research interests include virtual reality, digital geometry processing and computer-aided geometric design.

SHU LIU received a BSc degree in Mathematics from Zhejiang University in 2005. He is currently an MSc candidate in Applied Mathematics at Zhejiang University. His research interests span the fields of computer vision and computer graphics.

QUNSHENG PENG was born in 1947. He received a Ph.D. from University of East Anglia in 1983 and is currently a professor at the State Key Lab. of CAD & CG, Zhejiang University, People's Republic of China. His research interests include virtual reality, realistic image synthesis, infrared image synthesis and computer animation, and scientific visualization.